European Ice Sheet Modelling Initiative (EISMINT) model intercomparison experiments with first-order mechanics

Fuyuki Saito,[1,2] Ayako Abe-Ouchi,[1] and Heinz Blatter[3]

Received 9 December 2004; revised 31 January 2006; accepted 10 February 2006; published 2 June 2006.

[1] The European Ice Sheet Modelling Initiative (EISMINT) intercomparison experiments with thermomechanical coupling are repeated with an ice sheet model that applies the first-order approximation for computing the flow field. The experiments impose radially symmetric boundary conditions. Most of the previous results have shown the loss of implied radial symmetry, i.e., the formation of distinct, regularly spaced spokes of cold ice in the simulated basal temperatures. A similar result is also observed in the presented first-order model results. The computed velocity components scatter widely along the marginal grid points. This indicates that the spokes may be triggered by the poor representation of the margin with a regular grid, where the steep gradients in the surface enhance the numerical errors. Additionally, the generally applied second-order discretization scheme tends to decouple even and odd numbered grid points, thus leading to wavy solutions with a wavelength of two grid cells. These patterns strongly suggest that the loss in radial symmetry is a numerical artifact.

Citation: Saito, F., A. Abe-Ouchi, and H. Blatter (2006), European Ice Sheet Modelling Initiative (EISMINT) model intercomparison experiments with first-order mechanics, *J. Geophys. Res.*, *111*, F02012, doi:10.1029/2004JF000273.

1. Introduction

[2] The European Ice Sheet Modeling Initiative (EISMINT) intercomparison study addressed the effects of thermomechanical coupling with a series of experiments modeling an ice sheet with radially symmetric boundary conditions [*Payne et al.*, 2000]. A striking result is the loss of radial symmetry in a range of low temperatures, which was further discussed by *Payne and Baldwin* [2000]. Similar results were presented by *Payne and Dongelmans* [1997] for rectangular ice sheets, which they called the phenomenon "self-organization," and by *Hulton and Mineter* [2000] for circular ice sheets, who even called it "self-organization in ice streams."

[3] Some features in the broken symmetry indicate numerical origin. The patterns are best visible in the distribution of basal temperature, where spokes of cold ice clearly follow the grid lines and reflect grid symmetries. In this paper, we collect arguments indicating a numerical origin of the broken symmetry and the consequent spoke fields of velocity components and temperature. Although this paper cannot present a rigorous proof that the patterns are numerical artifacts, it seems timely to present strong arguments against physical interpretations of the spokes put forward so far in the four papers mentioned above, which presented little considerations of the numerical evidence. This paper collects evidence from numerical experiments that strongly support the assumption of a numerical origin of the observed patterns. A deeper mathematical analysis of the given set of equations and the applied numerical methods, and a possible solution to avoid the instabilities lie beyond the scope of this paper.

[4] All of the models used in the four previous studies cited above applied the zeroth-order shallow ice approximation [*Huybrechts*, 1992; *Greve*, 1997; *Saito and Abe-Ouchi*, 2004], where the velocity field is treated as a locally defined shear flow, and normal stress gradients are neglected. For some of the experiments presented in this paper, we used an ice sheet model that includes the effects of normal stress gradients [*Blatter*, 1995], sometimes called an incomplete second-order approximation [*Baral et al.*, 2001], which is hereafter referred to as first-order approximation (FOA). However, similar spokes appear in both types of approximations, indicating an origin from more basic conditions inherent in the numerical approach to be solved.

[5] In section 2, an account of the differences between the shallow ice and the first-order approximation and the applied boundary conditions is given. In section 3, we present results for different grid resolutions and different basal temperatures resulting from different surface and basal conditions, and for model experiments with and without thermomechanical coupling and with fixed surface geometries. An analysis of possible errors and error propagation presented in section 4 indicates a possible source for the

[1] Center for Climate System Research, University of Tokyo, Kashiwa, Japan.
[2] Now at Frontier Research Center for Global Change, Japan Agency for Marine-Earth Science and Technology, Yokohama, Japan.
[3] Institute for Atmospheric and Climate Science, Eidgenössische Technische Hochschule Zurich, Zurich, Switzerland.

0148-0227/06/2004JF000273$09.00

spokes at the boundary of the domain, which is poorly represented by the regular quadratic grid. Section 5 summarizes and discusses the various arguments supporting the hypothesis of a numerical origin of the spoke patterns in circular thermomechanically coupled ice sheet models using finite differences on regular grids.

2. Model Experiment Setup

[6] The zeroth-order shallow ice approximation (SIA) ice sheet model used in this study corresponds to the models described in detail by *Payne et al.* [2000]. A comprehensive description of the SIA is given by *Greve* [1997]. The model in the FOA deviates from these models mainly in the computation of the flow field and the strain heating. The FOA velocity and stress fields are computed with the method presented by *Blatter* [1995] and consider the gradients of normal stress components and horizontal shear stress. A detailed description of the coupled model used here is given by *Saito et al.* [2003]. The models contain two prognostic equations for the temperature and the surface, which depend on time t, and steady state equations for stress and flow fields. The horizontal spatial variables are x and y, and the vertical variable is z, the ice thickness $H = H(x, y) = S(x, y) - B(x, y)$, where S and B are the ice surface and base, respectively.

[7] The evolution of the local ice thickness H is determined by the local mass balance $M = M(x, y, t)$ and the local horizontal mass flux divergence, $\nabla_H \cdot \mathbf{f}$,

$$\frac{\partial S}{\partial t} = M - \nabla_H \cdot \mathbf{f} \equiv M - \frac{\partial (H\bar{u})}{\partial x} - \frac{\partial (H\bar{v})}{\partial y} \ , \tag{1}$$

where $\bar{u}$ and $\bar{v}$ are the vertically averaged horizontal velocity components. In the SIA, the terms $\bar{u}$ and $\bar{v}$ can be reduced to quadratures, whereas in the FOA, they must be computed directly by averaging velocity components obtained from the integration of the FOA equations for the horizontal velocity components.

[8] The horizontal velocity vector in the shallow ice approximation can be calculated by

$$\vec{v}_H = -2(\rho_I g)^n \left[\left(\frac{\partial S}{\partial x} \right)^2 + \left(\frac{\partial S}{\partial y} \right)^2 \right]^{\frac{n-1}{2}} \nabla_H S \int_B^z A(T)(S - z')^n \, dz', \tag{2}$$

where $g = 9.81$ m s^{-1} is the acceleration of gravity, $\rho_I = 910$ kg m^{-3} the density of ice. The basal sliding velocity is neglected in the present paper.

[9] The first-order force balance [*Blatter*, 1995] is

$$2\frac{\partial \sigma_{xx}}{\partial x} + \frac{\partial \sigma_{yy}}{\partial x} + \frac{\partial \tau_{xy}}{\partial y} - \rho_I g \frac{\partial S}{\partial x} + \frac{\partial \tau_{xz}}{\partial z} = 0, \tag{3}$$

$$2\frac{\partial \sigma_{yy}}{\partial y} + \frac{\partial \sigma_{xx}}{\partial y} + \frac{\partial \tau_{xy}}{\partial x} - \rho_I g \frac{\partial S}{\partial y} + \frac{\partial \tau_{yz}}{\partial z} = 0, \tag{4}$$

where σ_{ii} denotes the normal deviatoric stress components in the corresponding directions, τ_{ij} denotes the corresponding shear stress components, ρ_I and g are the density of ice and the acceleration of gravity, respectively. The FOA force balance contains not only the gradients of vertical shear stress components τ_{xz} and τ_{yz}, but also the normal deviatoric stress and horizontal shear stress components σ_{xx}, σ_{yy} and τ_{xy}.

[10] The first-order constitutive equations (Glen's flow law) are

$$\frac{\partial u}{\partial x} = A(T)\tau^{n-1}\sigma_{xx}, \tag{5}$$

$$\frac{\partial v}{\partial y} = A(T)\tau^{n-1}\sigma_{yy}, \tag{6}$$

$$\frac{1}{2}\frac{\partial u}{\partial z} = A(T)\tau^{n-1}\tau_{xz}, \tag{7}$$

$$\frac{1}{2}\frac{\partial v}{\partial z} = A(T)\tau^{n-1}\tau_{yz} \ , \tag{8}$$

$$\frac{1}{2}\left[\frac{\partial u}{\partial x} + \frac{\partial v}{\partial y}\right] = A(T)\tau^{n-1}\tau_{xy} \ , \tag{9}$$

where u, v are the horizontal velocity components in the x and y directions, respectively,

[11] The second invariant of the deviatoric stress tensor, τ, in the first-order approximation is

$$\tau^2 = \frac{1}{2}\mathrm{tr}[\sigma \cdot \sigma] = (\sigma_{xx})^2 + (\sigma_{yy})^2 + \sigma_{xx}\sigma_{yy} + (\tau_{xy})^2 + (\tau_{yz})^2 + (\tau_{zx})^2. \tag{10}$$

[12] Velocity fields are calculated for given surface and bottom topographies by the method of *Blatter* [1995] with equations (4), (9) and (10). Then, the local horizontal mass flux is obtained by vertical integration of the velocity fields, from which the evolution of the local ice thickness is determined.

[13] Velocity and temperature fields are coupled through the rate factor $A(T)$. An Arrhenius relation is used for calculation of $A(T)$:

$$A(T') = a \exp\left[\frac{-Q}{RT'}\right], \tag{11}$$

where $T' = T - T_{\mathrm{pm}} + T_0$ is absolute temperature corrected for the dependence of melting temperature T_{pm} on pressure and $T_0 = 273.15$ K is the triple point of water. Parameters a and Q follow the relations used by *Payne et al.* [2000].

[14] Temperature distribution is calculated from the thermodynamic equation under prescribed surface temperature and geothermal heat flux as boundary conditions:

$$\frac{\partial T}{\partial t} = \frac{k_I}{\rho_I c_p}\nabla \cdot \nabla T - (\vec{v} \cdot \nabla)T + \frac{\Phi}{\rho_I c_p}, \tag{12}$$

Table 1. Values of Climatic Boundary Conditions Used in the Different Numerical Experiments

Experiment	$M_{\max}$, m yr^{-1}	$T_{\min}$, K	S_T, K km^{-1}
A	0.5	238.15	1.67×10^{-2}
F	0.5	223.15	1.67×10^{-2}
C	0.05	223.15	4.175×10^{-3}

where $k_I = 2.1$ W m^{-1} K^{-1} and $c_p = 2009$ J kg^{-1} K^{-1} are thermal conductivity and specific heat capacity of ice, respectively, and Φ is the strain heating, which in the first-order approximation is

$$\Phi = \frac{\partial u}{\partial z}\tau_{xz} + \frac{\partial v}{\partial z}\tau_{yz} + \left(2\frac{\partial u}{\partial x} + \frac{\partial v}{\partial y}\right)\sigma_{xx} + \left(2\frac{\partial v}{\partial y} + \frac{\partial u}{\partial x}\right)\sigma_{yy} + \left(\frac{\partial u}{\partial y} + \frac{\partial v}{\partial x}\right)\tau_{xy}. \quad (13)$$

In the SIA, only the first two terms on the right hand side of equation (13) are included. At the surface of the ice, prescribed temperatures are employed. At the bottom of ice, the mixed boundary conditions are employed as follows:

$$\left.\frac{\partial T}{\partial z}\right|_B = -\frac{\Gamma}{k_I} \quad (14a)$$

if no melting and

$$T_B = T_{\text{pm}} \quad (14b)$$

if melting, where Γ is the prescribed geothermal heat flux.

3. Results

[15] The experiments, called experiments A0 and F0 with the SIA, and experiments A1 and F1 with the FOA, were performed using the same boundary conditions as the corresponding experiments A and F in the EISMINT model intercomparison experiments [*Payne et al.*, 2000]. The experimental design is as follows: The boundary conditions at the base of the ice sheet are no-slip condition and match the geothermal heat flux. However, temperature is constrained such that it does not exceed the local pressure melting temperature. The surface temperature T_s and mass balance M are given as functions of the horizontal distance R to the summit,

$$T_{\text{surface}} = T_{\min} + S_T R, \quad (15)$$

$$M = \min[M_{\max}, S_b(R_{\text{el}} - R)], \quad (16)$$

where $T_{\min}$ and S_T are the surface temperature at the summit and the radial surface temperature gradient, $M_{\max}$, S_b and R_{el} are upper limits for the accumulation rate, the radial mass balance gradient and the radial distance of the equilibrium line from the summit, respectively. The parameters in equations (15) and (16) are set as $S_b = 10^{-2}$ m yr^{-1}km^{-1}, $R_{\text{el}} = 450$ km in both experiment A and F. The climatic boundary conditions for experiments A and F are listed in Table 1 and the geothermal heat flux is set at 42 mW m^{-2} in all model experiments. The grid resolution is 25 km in both horizontal coordinate directions and the time step is 5 years for the surface evolution and the velocity field, and 25 years for the temperature field.

[16] Experiment A1 started with the steady state result of experiment A0 of the shallow ice approximation of the model (Figure 1a). The four initial spokes in the basal temperature distribution disappeared within about 50 kyr, and the circular symmetry was restored (Figure 1b). This seems to be not unexpected, since four out of 10 shallow ice models produced results of experiment A which are close to circular symmetry [*Payne et al.*, 2000].

[17] Several experiments with the first-order model were carried out using the boundary conditions of experiment F, however, with different initial conditions. The first experiment $F1_0$ started with the steady state solution of experiment F0 in the shallow ice approximation (Figure 1c). The first-order steady state shows similar spokes, which are aligned along the grid lines (Figure 1d). A second experiment $F1_A$ started with the circularly symmetric steady state of experiment A1 (Figure 1e). As soon as the temperature began to decrease, the spokes started to develop again. The pattern of steady state spokes in experiment $F1_A$, however, is different from the pattern of experiment $F1_0$. This demonstrates the possibility of multiple steady states for the same boundary conditions depending on the initial conditions.

[18] In one experiment C (Table 1), the surface boundary conditions for temperature are chosen such that the entire bed becomes cold. In this case the spokes disappear (Figure 1f), and circular symmetry is restored except for some irregularities along the ice margin, which are related to the coarse grid.

[19] Two experiments F started with the steady state of experiment $F1_A$, but this steady state was rotated by 45° and 30° around the origin. The spoke pattern disappeared after about 10 kyr and after a short transient state of relatively smooth temperature distributions, the spokes reappeared and developed into a steady state, which is close to the steady state of experiment $F1_A$.

[20] Experiments A0 and F0 were repeated with higher grid resolution, both with 12.5 km and 5 km (Figure 2). In the case of A0, the spokes along the coordinate axes become smaller with higher grid resolution (Figures 1a, 2a and 2b). The opposite occurs in experiment F0, where the spokes become more pronounced at higher resolutions (Figures 1c, 2c, and 2d). Because of extremely slow convergence of the iteration scheme, the higher-resolution experiments could not be performed with the first-order model.

4. Error Analysis

[21] In ice sheet models, surface evolution and velocity fields are computed in routines called in a cycle for each time step. For a given geometry, first the horizontal component of the velocity field and mass flux, secondly the vertical component of the velocity field and the consequent mass flux divergence, and thirdly, the surface evolution are computed. In thermomechanically coupled models, the temperature field is updated after a given number of time steps. In this section, the sensitivities of the single steps to perturbations are estimated.

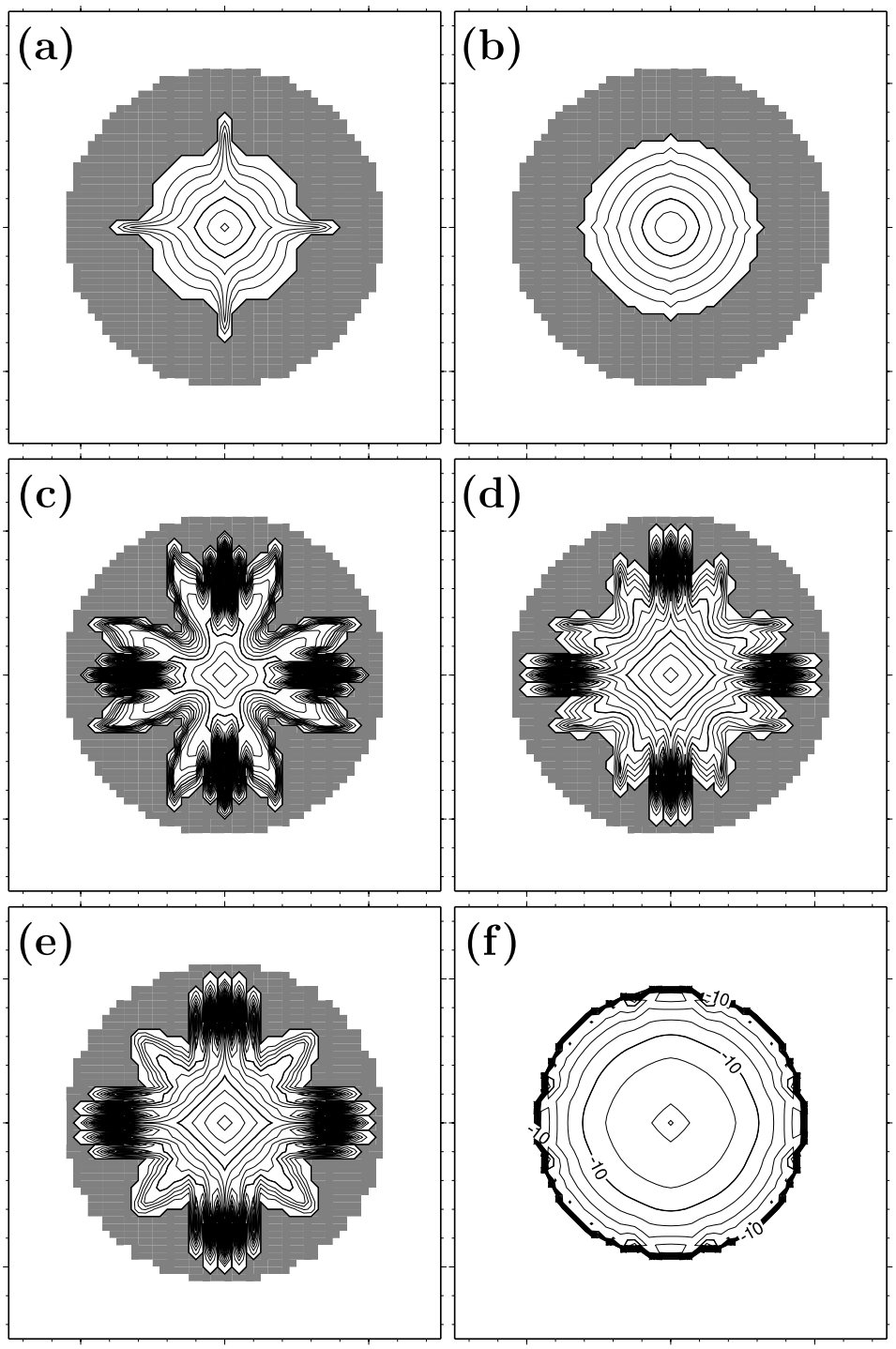

Figure 1. Steady state solutions of basal temperature below pressure melting point obtained by experiments (a) A0, (b) A1, and (c) F0. (d) Experiment $F1_0$ starting with the steady state solution of experiment F0 and (e) experiment $F1_A$ starting with the steady state solution of experiment A1. (f) Experiment C1. Shaded area indicates that the base is at pressure melting point. Contour interval is 2K for Figures 1a–1e and 0.5K for Figure 1f.

4.1. Mass Flux

[22] The mass flux $\bar{u}$ in the parallel sided slab is

$$\bar{u} = \int_B^S u(z')\mathrm{d}z' \propto (\rho g \sin\alpha)^3 (S-B)^5. \tag{17}$$

Relative errors (perturbations) in the thickness, H, and in the inclination, $\sin\alpha$, are transformed to a relative error $\delta\bar{u}/\bar{u}$ in the mass flux,

$$\frac{\delta\bar{u}}{\bar{u}} = 5\frac{\delta H}{H} + 3\frac{\delta(\sin\alpha)}{\sin\alpha}. \tag{18}$$

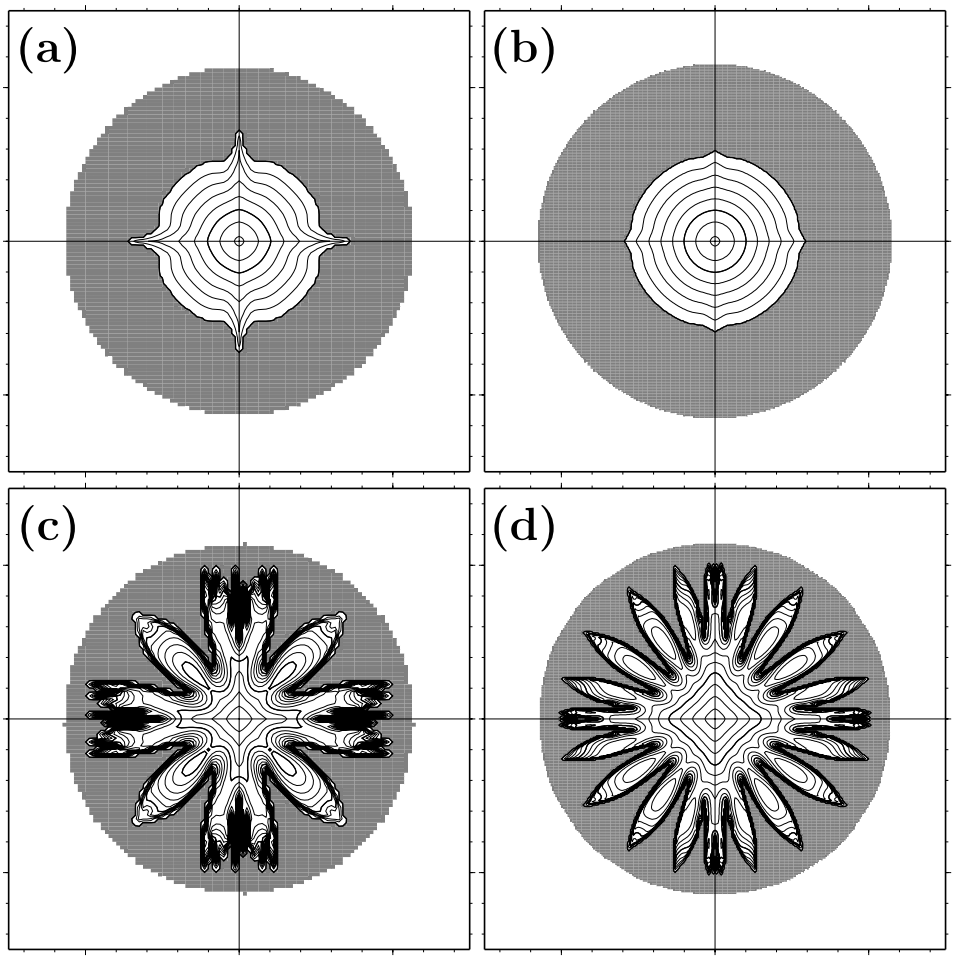

Figure 2. Steady state solutions of basal temperature below pressure melting point obtained by experiment A0 with (a) 12.5 km grid resolution and (b) 5 km resolution and by experiment F0 with (c) 12.5 km grid resolution and (d) 5 km resolution. Shaded area indicates that the base is at pressure melting point. Contour interval is 2 K.

[23] The errors are smaller in the first-order approximation, since the velocity vectors are not defined alone by the local ice thickness and surface inclination, but by their values in a neighborhood of about 5 to 10 ice thicknesses [*Paterson*, 1981].

4.2. Vertical Velocity and Mass Flux Divergence

[24] The generally used method to compute the vertical component of the ice velocity at the surface is derived by integrating the continuity equation of mass conservation,

$$w(x,s) = -\frac{\partial}{\partial x}\int_B^S u\mathrm{d}z' \equiv -\frac{\partial(H\bar{u})}{\partial x}. \tag{19}$$

[25] For a given horizontal component of the velocity field, u, and the surface geometry, S, the accuracy of the integration scheme is second order in the discrete element Δz, assuming numerical quadrature is performed with a second-order scheme. In a numerical scheme using finite differences, this yields

$$w_s = -\frac{\partial(H\bar{u})}{\partial x} \approx -\frac{\Delta H}{\Delta x}\bar{u} - H\frac{\Delta\bar{u}}{\Delta x}. \tag{20}$$

[26] This computation turns out to be very sensitive to perturbations or errors in u as well as $\Delta H/\Delta x$. The term $\Delta H/\Delta x$ is influenced by numerical error due to the marginal slope singularities. Besides, if we assume that the error δw only stems from errors $\delta\,(\Delta\bar{u})$ in the difference $\Delta\bar{u}$ of horizontal components of the velocity, u,

$$\delta w = \frac{\partial w}{\partial(\Delta\bar{u})}\delta(\Delta\bar{u}) = \frac{H}{\Delta x}\,\delta(\Delta\bar{u}). \tag{21}$$

[27] To estimate the magnitude of δw, we introduce the aspect ratio $\epsilon \equiv \hat{H}/\hat{L}$, where and $\hat{L}$ are the typical magnitudes of vertical and horizontal extents of the glacier, respectively. Furthermore, it is assumed that $\epsilon = \hat{W}/\hat{U}$, where $\hat{U}$ and $\hat{W}$ are the typical magnitudes of horizontal and vertical ice velocity at the ice surface. The length of the glacier is discretized with N grid cells of length $\Delta x = \hat{L}/N$, and thus from equation (21) we get

$$\frac{\delta w}{\hat{W}} \propto N\,\frac{\delta(\Delta\bar{u})}{\hat{U}}. \tag{22}$$

[28] Since $\Delta\bar{u}$ can be relatively small, the accuracy of this difference may suffer from digit elimination, especially if $\Delta\bar{u}$ is of the same order of magnitude as the individual errors $\delta\bar{u}$ of the mean velocities $\bar{u}$. In other words, we need

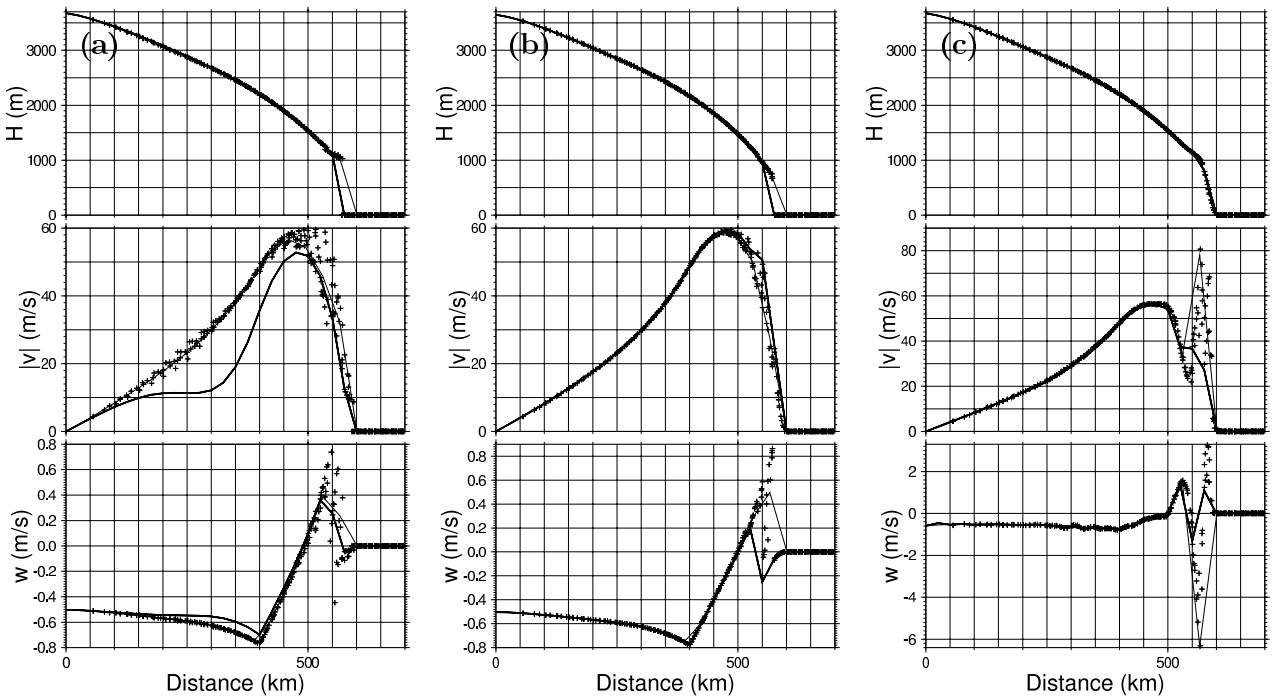

Figure 3. (top) Surface elevation, (middle) radial surface ice velocity component, and (bottom) vertical surface velocity component as a function of distance to the center of the ice sheet for (a) experiment A0 (basal temperature is shown in Figure 1a), (b) experiment A0 without thermomechanical coupling, and (c) experiment A0 with prescribed fixed surface geometry corresponding to the steady state solution of experiment A0 along the diagonal line $x = y$. The thick lines give the profile along the x and y coordinate axes, and the thin line along the diagonal is $x = y$. The crosses show the corresponding values on all other grid points.

to differentiate u numerically in order to compute w, and numerical differentiation is not well posed in the limit of taking small divided differences. This result is rather discouraging. Higher accuracy cannot be achieved by using higher-resolution Δx. The best accuracy lies somewhere between too high a resolution, where digit elimination becomes damaging, and too low a resolution, where the discretization error becomes too large. In any case, the relative error in the computed vertical velocity component is a multiple of the relative error in the computed or modelled horizontal velocity component.

4.3. Surface Evolution

[29] In most glacier and ice sheet models, the surface evolution is computed by converting equation (1) into a diffusion equation [*Huybrechts*, 1992] to achieve better numerical stability [*Hindmarsh and Payne*, 1996]. Stable solutions tend to smooth variations in the surface geometry if the mass flux distribution is smooth. A local perturbation thus delivers a wave along the surface with temporally decreasing amplitude and increasing wavelength. This smoothing tendency is often used to spin-up ice sheet model runs if the prescribed starting geometry is a measured surface topography [*Huybrechts*, 1992; *Calov and Hutter*, 1996; *Greve*, 1997].

[30] Within the described cycle of computation of the dynamics of an ice mass, the computation of the surface evolution is the only stabilizing part. It seems that in most cases the stabilizing effect is strong enough to restrain the other nonsmoothing effects.

4.4. Source of Errors

[31] If the surface slope is known exactly, the horizontal velocity field in the shallow ice approximation can be computed analytically, which will be well posed problem except where slope singularities occur. However, since the margin of the ice sheet is poorly represented by the regular quadratic grid, ill-conditioning appears in calculating the surface slope due to numerical differentiation[*Reist*, 2005]. To demonstrate the ill-conditioning of the numerical calculation of the velocity field near the margin, the surface velocity components at all grid points are plotted against the distance from the center of the ice sheet (Figure 3). Three different experiments for the warm thermal conditions are shown. The first case corresponds to the steady state of experiment A0 with thermomechanical coupling and calculated steady state surface (Figure 3a). In the second case (Figure 3b), the computed velocity field is not coupled to the thermal conditions and uses a prescribed flow rate factor corresponding to the steady state of experiment A0. The temperature field is computed using the uncoupled advection, however, strain heating is considered. In the third case, ice flow and temperature fields are coupled, but a fixed surface corresponding to the steady state solution of experiment A0 is prescribed (Figure 3c).

[32] In all of the cases, the radial (horizontal) and moreover, the vertical velocity component show a large scatter

near the ice margin. This confirms the prediction of equations (18) and (21), where relative errors in the velocity are multiples in the relative error of the ice thickness, and relative errors in the vertical velocity component are multiples of the relative errors in the horizontal velocity components. The latter is most clearly shown in the case of uncoupling thermal and mechanical conditions (Figure 3b). The thermomechanical coupling seems to enhance the sensitivity to perturbations and, in this case, already leads to small spokes in the temperature distribution. The marginal scatter becomes much larger in the case of prescribed ice surface. Even when the ice sheet geometry is fixed through time, there is a large scatter in the horizontal and vertical components of the velocity near the ice margin (Figure 3c). This outcome reflects the well known ill-conditioning of the given problem, namely numerically computing the vertical component of the velocity field for an ice surface prescribed on a grid [*Calov*, 1994].

5. Discussion

[33] The loss of radial symmetry is most pronounced in the ice temperature distribution, which is represented in graphs of the basal temperature (Figures 1 and 2). The loss of radial symmetry is characterized by some patterns which are common to all solutions.

[34] First, the solutions reflect the symmetry of the discretization grid. If the spoke patterns are solutions of the system of equations, then a rotated state is also a solution of the equations. Starting an experiment with a rotated solution does not yield rotated results (not shown here). The initial state quickly smooths and the solution returns to the spokes. The convergence toward a spoke solution aligned with the grid clearly indicates a strong influence of the numerical discretization scheme.

[35] Second, the poor representation of the margin by the regular quadratic grid seems to be particularly serious since surface gradients are steep near the singularity at the margin [*Fowler*, 2001]. Thus, they vary strongly due to the variable distance of the marginal grid points to the circular terminus expected for the ice sheet. Numerical results for velocities still scatter for solutions in which the circular symmetry is not broken (Figure 3). This indicates that the spokes may be triggered at the margin in cases where the stabilizing effect of the computation of the surface evolution is not strong enough to compensate the ill-conditioning of the computation of the velocity components with the zeroth and first-order shallow ice approximation. The ill-conditioning may be supported by the slope singularities at the margins in the actual underlying partial differential equations of the zeroth-order shallow ice approximation [*Fowler*, 2001], which cannot be handled by finite difference schemes that approximate gradients through polynomial interpolation. In addition, the coordinate transformation applied in most ice sheet models, mapping the local ice thickness onto unity, is also singular at the margin of the modeled domain.

[36] Third, all results have a common pattern as the spokes mirror the principal symmetries of the grid centered at the origin of the coordinate axes. Furthermore, the spokes always follow grid lines, and a section across the bundles of spokes reflects an oscillation pattern with a wavelength of exactly two grid cells. Such wavy patterns may be caused by partial numerical decoupling of solutions on even and odd numbered grid points. Figure 4 shows graphs of the basal ice temperatures of the shallow ice experiment F0 and of the first-order experiment $F1_0$, split into two parts. One part corresponds to the solution on the grid points with even numbers in both horizontal directions, the other part on the corresponding odd-numbered grid points. Both partial solutions are much smoother than the overall solution. Some smoother spokes remain and still reflect the symmetry of the grid. The solutions of all experiments show a similar pattern (not shown here), and the solutions on the even numbered grid points, which contain the coordinate axes, seem to display more pronounced spokes than the odd numbered solutions.

[37] This pattern is a clear fingerprint of a partial numerical decoupling between the even and odd numbered grid points. In a system of coupled equations, this decoupling may be amplified. Using a numerical solution of one equation for parts of the discretization of another equation may propagate this decoupling through the whole system of equations and their numerical solutions, and furthermore, may reduce the order of accuracy of the overall solution [*Colinge and Blatter*, 1998]. This may be the case by using the computed velocity field for the computation of the strain heating, and conversely, using the computed temperature field for computing the viscosity (rate factor) of the ice. A possible partial remedy may be the use of asymmetric higher-order difference schemes [*Colinge and Blatter*, 1998] or a multigrid method [*Briggs*, 1987; *Brandt*, 1977].

[38] The even-odd decoupling may be especially effective if large local gradients occur in the solution fields. This may be the case for polythermal situations where part of the base is cold and part of it is temperate. The local thickness of a possible basal layer of temperate ice may be quite sensitive to the local thermal and dynamical conditions [*Hutter et al.*, 1988]. The transition between the temperate and cold base along the spokes thus may become rather abrupt and may trigger the wavy pattern across the spokes as a result of the even odd decoupling. The poor representation of the margin by the regular grid additionally induces large transverse gradients along the ice edge, thus supporting the growth of the spoke patterns.

[39] Another question is raised by the fact that simulations of realistic ice sheets with the same thermomechanically coupled models do not result in similar spokes or wavy patterns. Perhaps the diffusive character of the numerical schemes is more effective in more irregular fields and helps to suppress the formation of spoke patterns, in contrast to the highly symmetric fields in the discussed circular geometry.

[40] It may be a difficult mathematical task to conclusively prove that the spoke patterns of the thermomechanically coupled solutions of the ice sheet equations are solely a numerical artifact. This argument may be supported by constructing a model with different discretization, either on a different coordinate system, e.g. cylindrical coordinates, or with an unstructured grid using finite elements. On the other hand, the character of the observed patterns strongly indicates their numerical origin, and it is premature to ascribe physical meaning to the spokes [*Hulton and Mineter*, 2000; *Payne and Dongelmans*, 1997]. It is certainly mandatory to first exclude all possibilities of

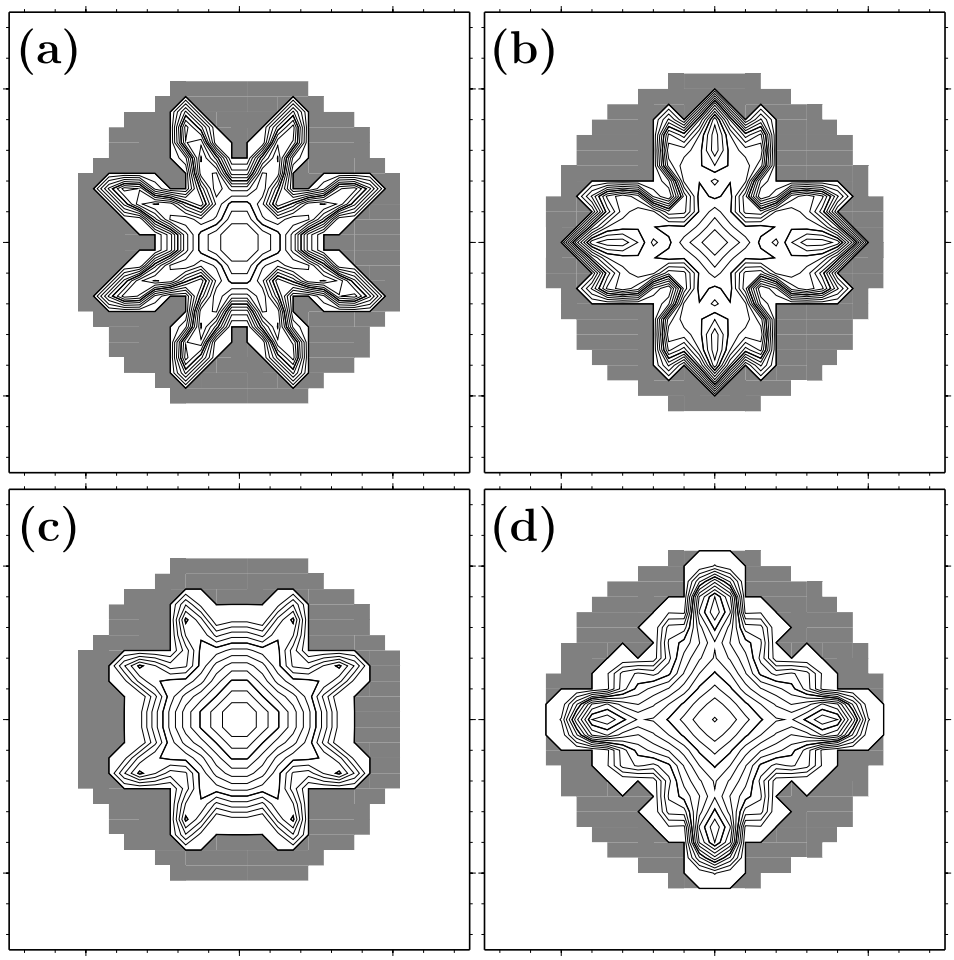

Figure 4. Steady state solutions of basal temperature below pressure melting point obtained by experiments (a and b) F0 and (c and d) $F1_0$ decomposed into two solutions: on even grid points (Figures 4a and 4c) and on odd grid points (Figures 4b and 4d). Shaded area indicates that the base is at pressure melting point. Contour interval is 2 K.

numerically induced errors and patterns before looking for physical interpretations of exotic patterns in model results.

[41] The question is whether the spokes are a result of ill-conditioning in the underlying equations, or a bad choice of discretization schemes and numerical algorithms. In the former case, no numerical algorithm can produce smooth solutions of the equations. In the latter case, an appropriate algorithm is required which can approximate the actual solutions. *Hindmarsh* [2004] concludes that there is an instability in the thermomechanical coupled shallow ice equations, which is ill posed. On the other hand, *Balmforth and Craster* [2000] present a well-posed streaming instability based on an asymptotic limit of rapid heat diffusion across a viscous layer for lava domes, however, the mathematics is the same as for ice sheets. *Hindmarsh* [2004] further discusses the mentioned instabilities of ice sheet flow and interprets them as instabilities of the physical system. The presented ''regime B'' fingering instabilities in the thermal conditions do not have a strong projection onto the ice thickness. This resembles to the EISMINT spokes. On the other hand, these spokes seem to be initiated at high slopes near the margin and propagate backwards into the ice sheet, corresponding to ''regime A'' instabilities [*Hindmarsh*, 2004]. If these physical instabilities exist and are critical for some wavelengths in perturbations, it may well be that the EISMINT spokes reflect this physical instability, but are caused by the wavelength of the grid. In this sense, the spokes may be both physical and numerical, although their strong two-grid wavelength is clearly forced by the grid and is thus numerical. If this is true, our arguments of the numerical origin of the spokes is both weakened and strengthened. The two grid wavelength is clearly numerical, but the existence of the spokes may reflect some physical background.

[42] **Acknowledgment.** The authors thank Will Sawyer, ETH Zurich, and the reviewers, Christian Schoof, University of British Columbia, and Frank Pattyn, Frije Universiteit Brussel, for careful and constructive reviews that helped to improve the paper substantially.

References

Balmforth, N. J., and R. V. Craster (2000), Dynamics of cooling domes of viscoplastic fluid, *J. Fluid Mech.*, *422*, 225–248.

Baral, D. R., K. Hutter, and R. Greve (2001), Asymptotic theories of large-scale motion, temperature, and moisture distribution in land-based polythermal ice sheets: A critical review and new developments, *Appl. Mech. Rev.*, *54*(3), 215–256.

Blatter, H. (1995), Velocity and stress fields in grounded glaciers: A simple algorithm for including deviatoric stress gradients, *J. Glaciol.*, *41*, 333–344.

Brandt, A. (1977), Multi-level adaptive solutions to boundary value problems, *Math. Comput.*, *31*, 333–390.

Briggs, W. L. (1987), *A Multigrid Tutorial*, Soc. for Ind. and Appl. Math., Philadelphia, Pa.

Calov, R. (1994), Das thermomechanisches Verhalten des Grönländischen Eisschildes unter der Wirkung verschiedener Klimaszenarien—Antworten eines theoretisch-numerischen Modells, Ph.D. thesis, Tech. Hochsch. Darmstadt, Darmstadt, Germany.

Calov, R., and K. Hutter (1996), The thermomechanical response of the Greenland ice sheet to various climate scenarios, *Clim. Dyn.*, *12*, 243–260.

Colinge, J., and H. Blatter (1998), Stress and velocity fields in glaciers: Part I. Finite difference schemes for higher-order glacier models, *J. Glaciol.*, *44*, 448–456.

Fowler, A. C. (2001), Modelling the flow of glaciers and ice sheets, in *Continuum Mechanics and Applications in Geophysics and the Environment*, edited by B. Straughan, et al., pp. 201–221, Springer, New York.

Greve, R. (1997), A continuum-mechanical formulation for shallow polythermal ice sheets, *Philos. Trans. R. Soc. London, Ser. A*, *355*, 921–974.

Hindmarsh, R. C. A. (2004), Thermoviscous stability of ice-sheet flows, *J. Fluid Mech.*, *502*, 17–40.

Hindmarsh, R. C. A., and A. J. Payne (1996), Time-step limits for stable solutions of the ice-sheet equation, *Ann. Glaciol.*, *23*, 74–85.

Hulton, N. R. J., and M. J. Mineter (2000), Modelling self-organization in ice streams, *Ann. Glaciol.*, *30*, 127–136.

Hutter, K., H. Blatter, and M. Funk (1988), A model computation of moisture content in polythermal glaciers, *J. Geophys. Res.*, *93*(B10), 12,205–12,214.

Huybrechts, P. (1992), The Antarctic ice sheet and environmental change: A three-dimensional modelling study, *Rep. Polar Res. 99*, Alfred-Wegener-Inst. für Polar- und Meeresforsch., Bremerhaven, Germany.

Paterson, W. S. B. (1981), *The Physics of Glaciers*, 2nd ed., Elsevier, New York.

Payne, A. J., and D. J. Baldwin (2000), Analysis of ice-flow instabilities identified in the EISMINT intercomparison exercise, *Ann. Glaciol.*, *30*, 204–210.

Payne, A. J., and P. W. Dongelmans (1997), Self-organization in the thermomechanical flow of ice sheets, *J. Geophys. Res.*, *102*(B6), 12,219–12,233.

Payne, A. J., et al. (2000), Results from the EISMINT model intercomparison: The effects of thermomechanical coupling, *J. Glaciol.*, *46*, 227–238.

Reist, A. (2005), Mathematical analysis and numerical simulation of the motion of a glacier, Ph.D. thesis, Ecole Polytech. Fed. de Lausanne, Lausanne, Switzerland.

Saito, F., and A. Abe-Ouchi (2004), Thermal structure of Dome Fuji and East Queen Maud Land, Antarctica, simulated by a three-dimensional ice sheet model, *Ann. Glaciol.*, *39*, 433–438.

Saito, F., A. Abe-Ouchi, and H. Blatter (2003), Effects of first-order stress gradients in an ice sheet evaluated by a three-dimensional thermomechanical coupled model, *Ann. Glaciol.*, *37*, 166–172.

A. Abe-Ouchi, Center for Climate System Research, University of Tokyo, 5-1-5 Kashiwanoha, Kashiwa, Chiba 277-8568, Japan.

H. Blatter, Institute for Atmospheric and Climate Science, Universitätstrasse 16, ETH Zurich, CH-8092 Zurich, Switzerland. (heinz.blatter@env.ethz.ch)

F. Saito, Frontier Research Center for Global Change, 3173-25 Showamachi, Kanazawa-ku, Yokohama, Kanagawa 236-0001, Japan. (saitofuyuki@jamstec.go.jp)